17th Brazilian Congress of Thermal Sciences and Engineering
November 25th-28th, 2018, Águas de Lindóia, SP, Brazil

ENCIT-2018-0166
PREDICTION OF HEAT TRANSFER COEFFICIENT DURING CONDENSATION OF R404a IN HELICALLY COILED TUBES USING ADAPTIVE NEURO-FUZZY INFERENCE SYSTEM

Ali Khosravi
Department of Mechanical Engineering, Aalto University, Helsinki, Finland
alikhosravii@yahoo.com

Juan J. G. Pabon
Institute of Mechanical Engineering, Federal University of Itajubá, Itajubá, Brazil
langa_27@hotmail.com

Túlio da Motta Corrêa
Luiz Machado
Graduate Program in Mechanical Engineering, Federal University of Minas Gerais, Belo Horizonte, Brazil
tuliodamotta@gmail.com; luizm@demec.ufmg.br

Abstract. *Condenser is an important heat exchanger widely used in refrigeration and air conditioning systems. Heat transfer coefficient (HTC) of two-phase flow of refrigerants is important in order to design a heat exchanger. In this study, Adaptive Neuro-Fuzzy Inference System (ANFIS) is developed to predict the HTC under condensation of R404a in a helically coiled tube. Particle Swarm Optimization (PSO) algorithm and Genetic Algorithm (GA) are used to optimize the ANFIS model. Vapor quality, mass flux of refrigerant, pitch and curvature radius are considered as input variables of the network and HTC is selected as its output variable. The results illustrate that using GA to optimize the ANFIS model improves correlation coefficient with approximately 8% and decreases the value of RMSE around 52% for testing datasets. Also, the ANFIS model optimized with PSO algorithm reports the best performance for the predicted HTC with correlation coefficient and MAPE respectively as 0.9876 and 1.35% for the testing datasets.*

Keywords: *ANFIS, particle swarm optimization, genetic algorithm, heat transfer coefficient, R404a*

1. INTRODUCTION

World energy consumption is increasing continually and this event is worrisome for all researchers and scientists (Faria *et al.*, 2016) . The increase in energy demand, depletion of fossil resources and environmental pollution problem have led to a growth of interest in more efficient systems (De Melo Reis *et al.*, 2012). Heat transfer is one of the main areas in energy field and takes place in many industrial and domestic applications (Goshayeshi *et al.*, 2014). The knowledge of heat transfer is essential in order to design a heat exchanger (Kumar and Kumar, 2016). One of the most important types of heat exchangers are condensers that are used in refrigeration systems, air-conditioning, and heat pump applications. Using the helically coiled tube in heat exchangers increases the efficiency of the heat exchangers (Salimpour *et al.*, 2017). Heat transfer in two-phase flow of any fluid is larger than single-phase flow (Huang and Thome, 2017). Hence many investigations were focused on the effect of different parameters in two-phase flow of refrigerants under evaporation and condensation processes such as diameter, vapor quality, mass flux and etc. (Diani *et al.*, 2015; Guo *et al.*, 2016; Belman-Flores *et al.*, 2017; Makhnatch *et al.*, 2017).

Due to the two-phase flow complexity, the prediction of HTC is mostly done with empirical correlations and need many experimental tests (Balachander *et al.*, 2012). But the fact is that the high non-linearity of the two-phase flow makes the cause-effect relation difficult to assimilate, and the exam of numerical methods to estimate and predict HTC has been frequently used (Gorenflo *et al.*, 2014). Artificial intelligent methods are defined as new methods to estimate the two-phase flow of HTC that create a non-linear relationship between the inputs to estimate the outputs. More importantly, the use of artificial intelligence methods to predict HTC in two-phase flow of refrigerants can significantly reduce the experiment period, test material and reduce the cost.

Azizi and Ahmadloo (2016) developed a multilayer perceptron (MLP) neural network to predict HTC during condensation of R134a in an inclined tube. Mass flux, inclination angle, saturation temperature and mean vapor quality were considered as input variables of the network and HTC was selected as the output variable. The optimal structure of the developed model was obtained with 18 neurons in the hidden layer. The network reported mean absolute percent error (MAPE) of 1.94% and correlation coefficient (R) of 0.995 for testing data.

Ma *et al.* (2017) proposed a backpropagation neural network for prediction of supercritical water HTC. The inputs variables of the network were considered as specific enthalpy, diameter, mass flux, heat flux, and pressure. The maximum performance of the network was obtained with 30 neurons in the hidden layer. It is found that the mean error, standard

deviation and root mean square error for the measured and predicted data are 0.18%, 4.12% and 0.18%, respectively. The prediction range of the network was determined as follow: mass flux is 400-3000 kg/m²s, specific enthalpy is 451.30-3135.87 kJ/kg, heat flux is 200-2960 kW/m², pressure is 22.6-31 MPa and the range of diameter is 0.7-38.1 mm.

Prediction of gas-liquid two-phase HTC was done by Ren *et al.* (2017). Forecasting model based on the last square support vector machine (LSSVM) was developed to forecast HTC. They used the group search optimizer (GSO) algorithm to find the optimal hyper-parameters in LSSVM technique. The results illustrated that the developed network can successfully predict the target with small samples and high accuracy.

Romero-Méndez *et al.* (2016) proposed an Artificial Neural Network (ANN) to estimate the convective HTC during the evaporation of refrigerant flowing inside mini-tube. An experimental setup was prepared to obtain the HTC data in R-134a refrigerant. Saturated temperature, mass flux and heat flux were considered as inputs of the network and HTC during two-phase flow of R-134a refrigerant was predicted. The maximum error and a mean quadratic error for the predicted HTC were obtained as 2.46% and 0.51%, respectively.

Wen *et al.* (2012) proposed a radial basis function (RBF) neural network to predict flow boiling HTC for R407C inside horizontal smooth tubes. Some factors strongly affecting the flow boiling of R407C that have been considered as inputs of the network. These factors are mass flux, heat flux, vapor quality, saturation temperature and tube inner diameter. The K-means clustering algorithm was used to design RBF network. To evaluate the network the average deviation, absolute average and root mean square deviations were considered that were reported to be -0.9%, 5.5% and 10.9%, respectively.

Hassanpour *et al.* (2018) implemented artificial intelligence (AI) approaches in order to predict pool boiling HTC of alumina water-based nanofluids. MLP, RBF, general regression (GR) and cascade feed-forward were considered as AI methods for prediction of pool boiling HTC. The models were designed with diameter of nanoparticles, its weight concentration in base fluid, excess temperature and operating pressure as inputs. Their results illustrated that MLP neural network is the best model to predict the target. For this network, the best performance was obtained with 12 neurons in the hidden layer. The network was able to predict the target with mean square error, MSE = 4.17, determination coefficient, $R^2 = 0.9929$ and root mean square error, RMSE = 2.042.

ANN was used to estimate HTC of two-phase flow of air-water in a horizontal pipe for different inclined positions by Sobhanifar *et al.* (2015). They considered the superficial liquid and gas Reynolds numbers and the inclination of the pipe as inputs and HTC of two-phase flow of air-water as target of the network. Multilayer feed-forward neural network was developed to estimate the targets. The range of superficial liquid and gas Reynolds numbers were considered from 740 to 26,100 and 560 to 47,600 for water and air respectively. The proposed network reported the mean relative error (MRE) of 2.92% and correlation coefficient (R) of 0.997 for all datasets.

This study concentrates on the prediction of HTC during condensation of R404a in helically coiled tubes. R404a is a suitable alternative for R22 refrigerant and it has an ozone depletion potential (ODP) equal to zero. Prediction of HTC of two-phase flow of R404a is done by developing an ANFIS model that is optimized with PSO and GA algorithms. To design the network, vapor quality, mass flux, pitch and curvature radius are selected as inputs of the network and HTC is the target. The data were divided into two samples as 70% for training and 30% for testing processes. For this purpose, experimental data reported by Salimpour *et al.* (2017) were used.

2. METHODOLOGY

2.1 Experimental setup

The goal of this study is to predict the HTC under condensation of R404a. This investigation is done for a shell and helical tube heat exchanger that is shown in Fig. 1. The heat exchanger contains a helically coiled tube which accommodates the condensing flow of R404a. A copper straight tube with length of 3.2 m was used to form the coiled tube. Table 1 represents the range of operating parameters. The inner diameter of the coiled tube is 7.52 mm. Also, the coiled tube is of 1 mm thickness, 8.7 to 15.3 cm coil diameter and 1.5 to 3.5 cm is considered for coil pitch.

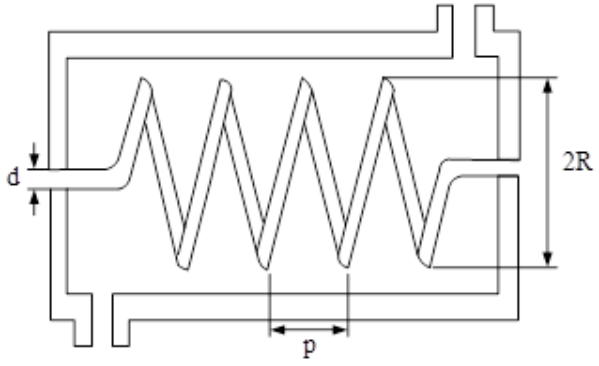

Figure 1. Shell and helical tube heat exchanger.

Table 1. Range of operating parameters.

Heat exchanger	d_i (mm)	d_o (mm)	R (cm)	p (cm)	L (m)
1	7.52	9.52	4.35	1.5	3.2
2	7.52	9.52	4.35	2.5	3.2
3	7.52	9.52	4.35	3.5	3.2
4	7.52	9.52	6.35	1.5	3.2
5	7.52	9.52	6.35	2.5	3.2
6	7.52	9.52	6.35	3.5	3.2
7	7.52	9.52	7.65	1.5	3.2
8	7.52	9.52	7.65	2.5	3.2
9	7.52	9.52	7.65	3.5	3.2

The range of operating conditions is shown in Tab. 2. The mass flow rate of refrigerant (R404a) changes from 125 to 188 kg/m²s. For this purpose, 162 test runs are performed. More details on experimental setup are found in Salimpour *et al.* (2017).

Table 2. Range of operating conditions.

Refrigerant mass velocity	125 – 188 kg/m²s
Average condensing temperature	29.1 - 39.1 °C
Average cooling heat flux	3.1 – 21 kW/m²
Cooling water mass flow rate	0.011 - 0.089 kg/s
Inlet temperature of cooling water	21.5 - 22.4 °C
Inlet vapor quality	0.24 - 0.85

2.2 Adaptive neuro-fuzzy inference system (ANFIS)

Fuzzy rules are obtained from the human expert in the most FIS systems, hence ANN was incorporated into a fuzzy system to obtain the knowledge of human expert by applying the learning algorithms (Quej *et al.*, 2017). This method was used for automatic fuzzy if-then rules generation. This connection (an ANN into fuzzy system) is called neuro-fuzzy system. The most frequently used ANN in neuro-fuzzy system is radial basis function neural network (RBFNN) in which each node has radial basis function such as Gaussian and Ellipsoidal. There are many developed neuro-fuzzy algorithms that adaptive neuro inference system is one of them. This algorithm uses RBFNN to determine the parameters of the fuzzy system. In this model Takagi–Sugeno–Kang models are involved in framework of adaptive system. ANFIS contains two main parameters that are defined as antecedent and consequent parameters. These two parameters connect the fuzzy rules to each other and training the network is provided with the optimization of these parameters. Figure 2 shows a basic ANFIS structure that consists of five layers with two inputs and one output.

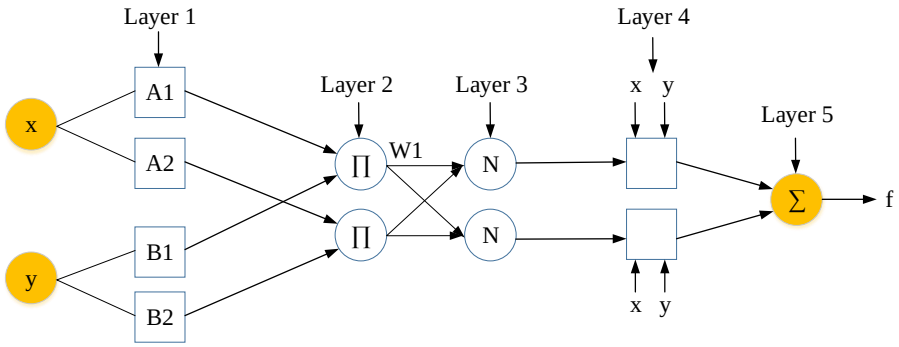

Figure 2. ANFIS structure

In the first layer, the signal that is achieved from each node is transferred to the other layer (this layer is called fuzzification layer). Equations (1) and (2) are given to describe the outputs of the cells (O_{1i}) in this layer (Haznedar and Kalinli, 2016).

$$O_{1,i} = \mu_{A_i}(x), \qquad i = 1,2 \tag{1}$$

$$O_{1i} = \mu_{B_{i-2}}(y), \qquad i = 1,2 \tag{2}$$

In which x is the input to node i, and $A_i(or\ B_{i-2})$ is a linguistic label (such as "small" or "large") associated with this node. Also, $O_{1,i}$ is the membership grade of a fuzzy set A and it specifies the degree to which the given input x satisfies the quantifier A. The membership function for A can be any appropriate membership function, such as the Triangular or Gaussian. When the parameters of membership function changes, chosen membership function varies accordingly, thus exhibiting various forms of membership functions for a fuzzy set A. Parameters in this layer are referred to as "premise parameters". For a Gaussian membership function, μ_{A_i} (is called membership degree) is obtained with the following equation:

$$\mu_{A_i} = e^{-\frac{1}{2}\left(\frac{x-c}{a}\right)^2}, \quad i = 1,2 \tag{3}$$

where a_i and c_i are sigma and central parameters of the membership function, respectively.

The second layer is called the rule layer that is obtained with the membership degrees that are coming from the first layer (each node output represents the firing strength of a fuzzy rule).

$$O_{2,i} = w_i = \mu_{A_i}(x).\mu_{B_i}(y), \quad i = 1,2 \tag{4}$$

The third layer is the normalization layer that every node in this layer is a fixed node labeled N. The ith node calculates the ratio of the rule's firing strength to the sum of all rules' firing strengths:

$$O_{3,i} = \overline{w}_i = \frac{w_i}{w_1 + w_2}, \qquad i = 1,2 \tag{5}$$

Layer 4 is the defuzzification layer in which output value for each rule is calculated from the value of previous layer.

$$O_{4,i} = \overline{w}_i f_i = \overline{w}_i(p_i x + q_i y + r_i), \quad i = 1,2 \tag{6}$$

in which $\overline{w}_i$ is a normalized firing strength from layer 3 and $\{p_i, q_i, r_i\}$ is the parameter set of this node. Parameters in this layer are referred to as "consequent parameters".

The last layer is the sum layer (layer 5). The output of ANFIS model is obtained by collecting the output values of each rule that are obtained in defuzzification layer.

$$O_{5,i} = f = \sum \overline{w}_i f_i = \frac{\sum w_i f_i}{\sum w_i}, \qquad i = 1,2 \tag{7}$$

2.3 Genetic Algorithm (GA)

Genetic Algorithm (GA) that has been introduced by John Holland in 1970, is a class of probabilistic optimization algorithms and inspired by the biological evolution process (Haznedar and Kalinli, 2016). This algorithm uses concepts of "Natural Selection" and "Genetic Inheritance". A simple structure of GA is shown in Fig. 3. It begins with random initiation of a population using chromosomes as abstract presentations of solution candidates. To initialize the GA, a population of individuals with random chromosomes is generated. During single iteration of the GA, individuals in the population compete for their right to reproduce, favoring those who maximize the value of a fitness function which customarily maps every individual to a single decimal value from the [0;1] interval. At the end of the iteration, fit individuals are selected and allowed to produce an offspring population, on which the next iteration of the GA operates. This behavior creates an iterative loop, which can be summarized by a diagram shown in Fig. 3.

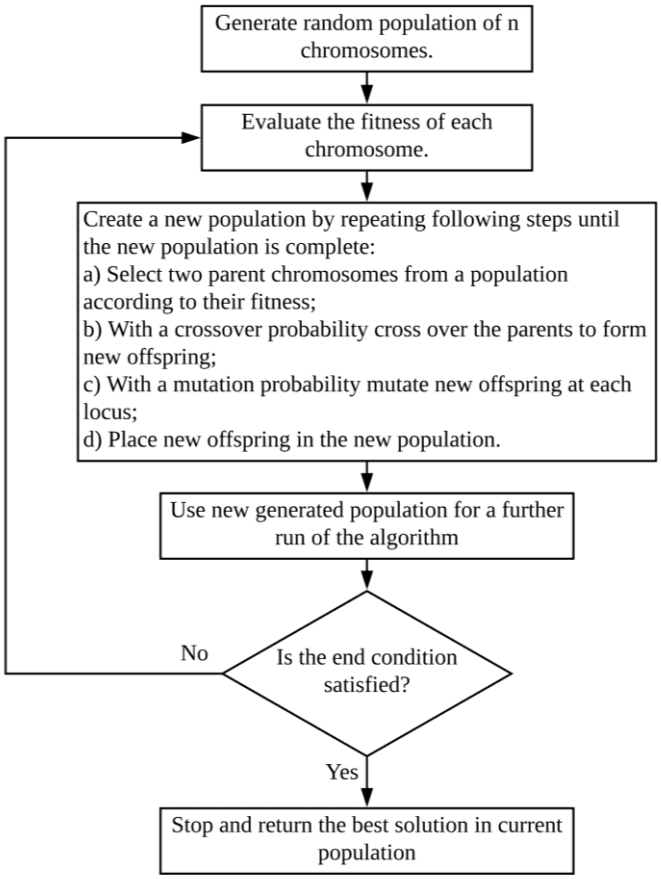

Figure 3. Design structure of genetic algorithm

2.4 Particle Swarm optimization (PSO)

Partial swarm optimization (PSO) that has been introduced by Russell Eberhart and James Kennedy in 1995. It inspired by the flocking and schooling patterns of birds and fish (Oliveira and Schirru, 2009). Every PSO uses a population of particles. The number of particles in a swarm is typically far less than the number of individuals in an evolutionary algorithm. A particle in this population is interconnected to other particles. This interconnection is called the neighborhood topology. Neighborhood refers to a communication structure rather than a geographical neighborhood. To use these particles to explore the search space we need a so-called change rule. This rule moves the particles through the search space at a given moment t in time depending on its position at moment $t-1$ as well as the position of its previous best location. This is the cognitive aspect of the PSO. The social aspect is introduced by an interaction rule. A particle's position is not only dependent on its own best position in history, but also on the best position in history of its neighbors.

In PSO algorithm each particle is composed of three N-dimensional vectors in which N is the dimensionality of the search space and a real-value:

- $\vec{x}_i$ the current position in the search space of particle i;
- $\vec{p}_i$ the best position in history of particle i;
- $\vec{v}_i$ the speed of particle i;
- Personal best i ($pBest_i$) the quality of the solution of the best position of particle i.

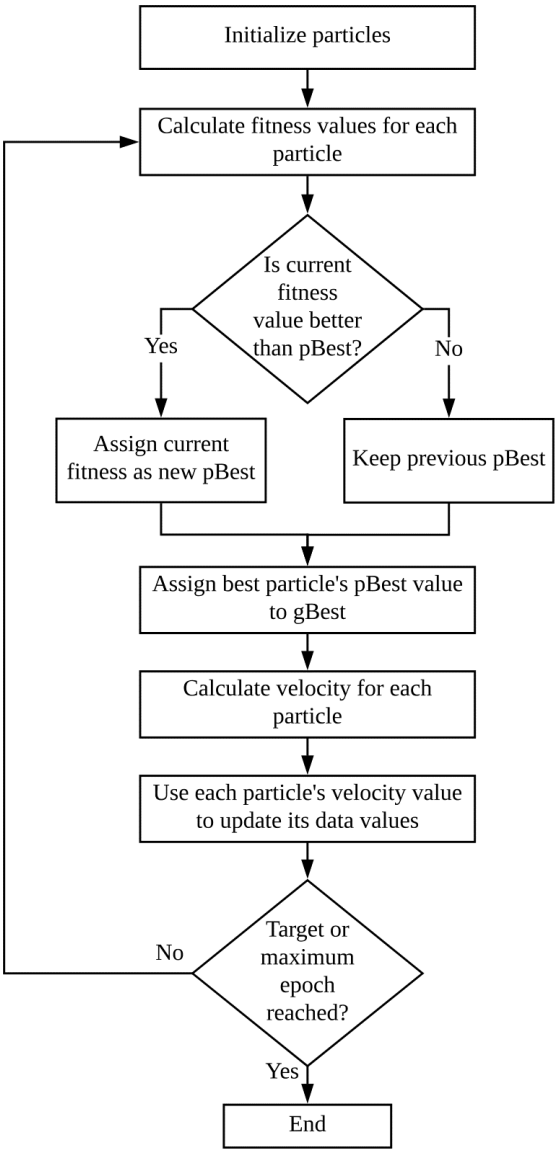

Figure 4. Design structure of particle swarm optimization algorithm

2.5 Training ANFIS using optimization methods

The ANFIS parameters are updated with the PSO and GA optimization algorithms. ANFIS has two main parameters that should be updated with the optimization algorithms that are premise and consequent parameters. The premise parameters are $\{a_i, c_i\}$ that belong to gauss membership function and are given in Eq. 3. The total number of these parameters is equal to the sum of the parameters in all membership functions. Consequent parameters are $\{p_i, q_i, r_i\}$ and are used in defuzzification layer and are given in Eq. 6.

3. RESULTS AND DISCUSSION

The developed ANFIS model is called ANFIS-FCM that uses fuzzy c-means clustering to determine the number of rules and membership functions for the antecedents and consequents. Figure 5 shows the structure of ANFIS model with four inputs and one output. Ten clusters are generated for each input with 10 rules.

Figure 6 represents the ANFIS decision surface for the HTC estimation using the two inputs (input 1: vapor quality and input 2: mass flux) and output (output: HTC). According to the decision surface, the maximum HTC is obtained for the highest value of vapor quality and mass flux.

The ANFIS decision structure for input 4 (pitch) and input 3 (curvature radius) with output (HTC) is shown in Fig. 7. The figure indicates that the maximal HTC occurs for minimal pitch and curvature radius. The decision surface shows the variation of HTC during two-phase flow of R404a in relation to the inputs.

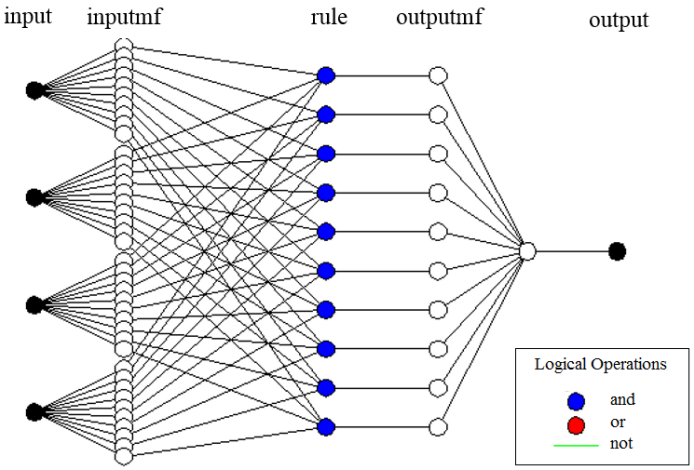

Figure 5. Structure of ANFIS model.

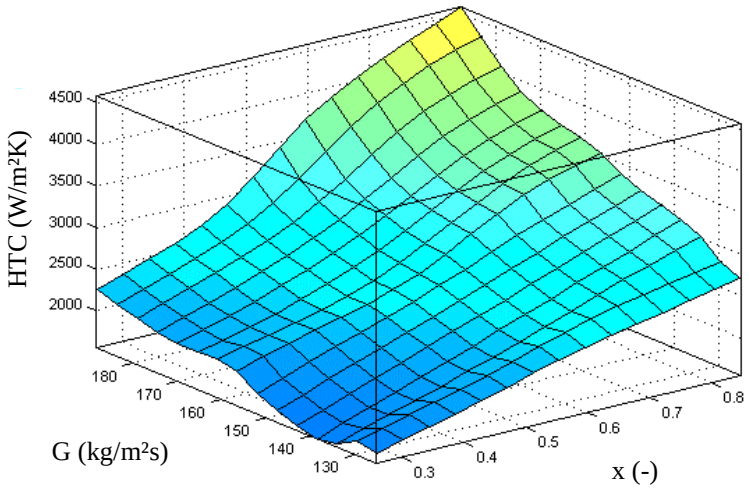

Figure 6. ANFIS decision surface for the HTC estimation.

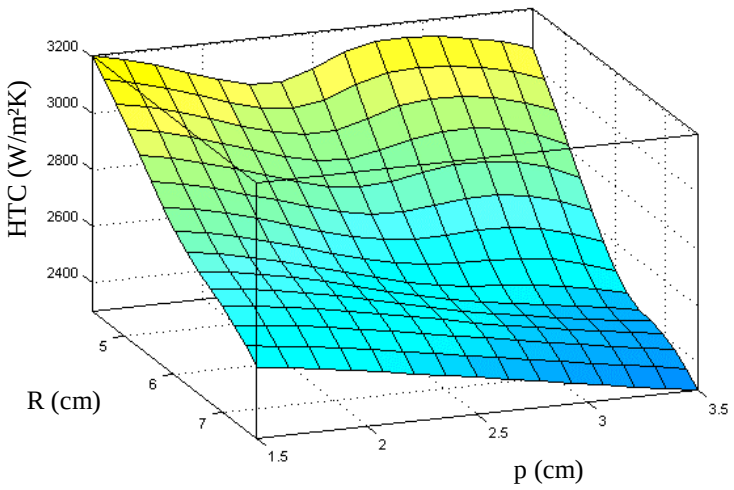

Figure 7. ANFIS decision surface for HTC prediction.

Table 3 shows three types of statistical parameters (root mean square error (RMSE), correlation coefficient (R) and mean absolute percentage error (MAPE)) that are applied to evaluate the predicted data for ANFIS model. These parameters are described in section 5 (Appendix). ANFIS (model-1) with 10 clusters reports the maximum performance of the model in terms of RMSE, R and MAPE to be 346.5004, 0.9077 and 6.12% for testing samples.

Table 3. Performance of the ANFIS model with different clusters.

		RMSE		R		MAPE	
Model	Clusters	Train	Test	Train	Test	Train	Test
1	10	38.1079	346.5004	0.9985	0.9077	0.88%	6.12%
2	15	16.7539	376.3213	0.9997	0.9065	0.21%	9.22%
3	20	2.8856	490.4904	1	0.8597	0.04%	10.56%

Figure 8 illustrates training and testing datasets and provides a comparison of the predicted HTC via the ANFIS model and the actual data (target data). For training datasets, the predicted data pattern is observed to follow the actual data pattern closely, with little disagreement. Testing the model with new samples shows the predicted HTC follows the experimental data with more disagreement compared to training phase of the network. For testing datasets, the correlation coefficient is obtained as 0.9077.

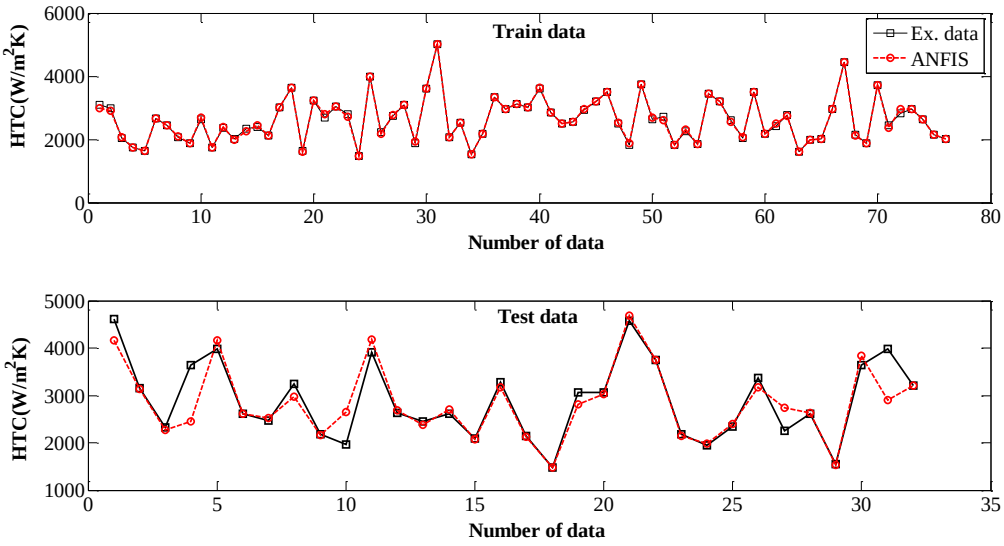

Figure 8. Training and testing datasets for the ANFIS model.

The premise and consequent parameters of ANFIS model are updated with the GA optimization algorithm. The number of clusters in ANFIS model is considered as 10 clusters. Also, the GA parameters selected are as follows: $n_{max} = 500$ (maximum iterations), $n_p = 100$ (number of population), crossover percentage is 0.7, mutation percentage is 0.5 and mutation rate is considered as 0.1. Figure 9 demonstrates the prediction of HTC under two-phase flow of R404a with ANFIS-GA (ANFIS that optimized with GA) agrees well with the experimental data. This model reports a correlation coefficient of R = 0.9801 for the testing dataset that is approximately 8% more than the ANFIS model.

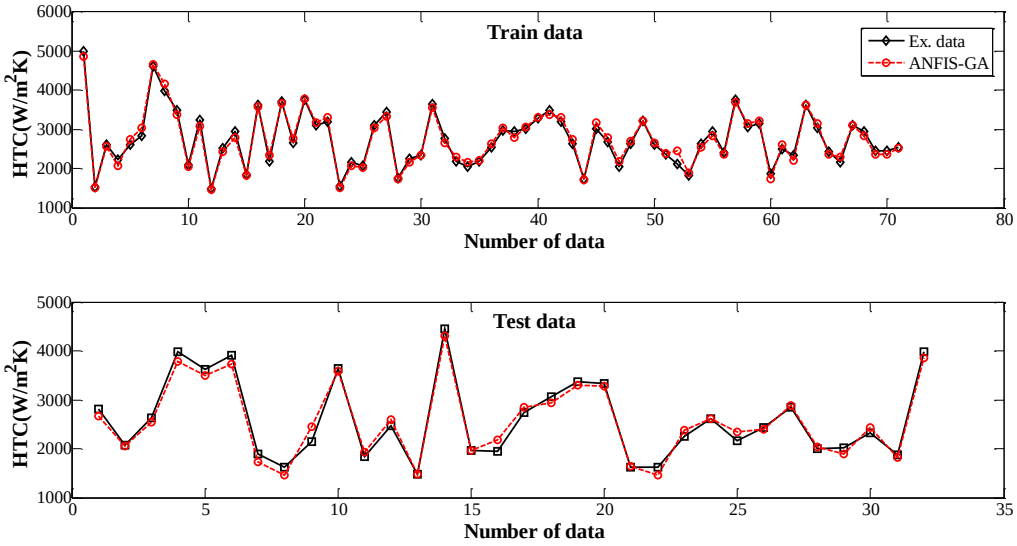

Figure 9. Training and testing samples for ANFIS-GA model.

Also, PSO algorithm is used to optimize the ANFIS parameters. The PSO parameters are selected as follows: the size of population is 20, the maximum iteration is 1500, $C_1 = 1$ (personal learning coefficient), $C_2 = 2$ (global learning coefficient) and inertia weight is considered as 1. Figure 10 demonstrates the predicted HTC data and experimental data with the ANFIS optimized by PSO model (ANFIS-PSO). The graph shows the predicted HTC agrees well with the target data and that the magnitude of the disagreement between the predicted and actual data is small. This model obtains the best performance to predict the HTC in terms of RMSE, R and MAPE, respectively with, 108.3395, 0.9876 and 1.35% for the test data.

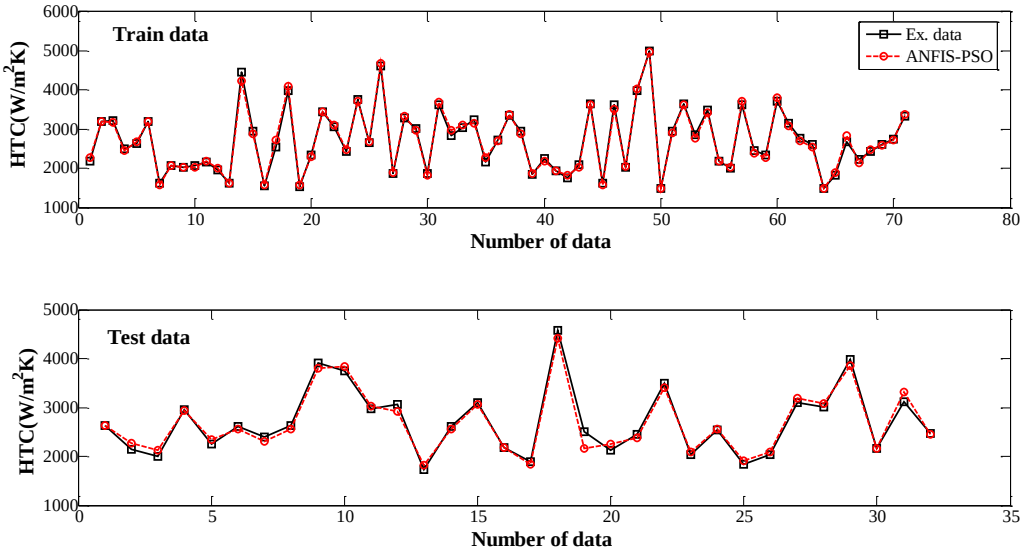

Figure 10. Prediction of HTC with ANFIS-PSO model (train and test data).

Table 4 compares the performance of the developed models in order to estimate the HTC during condensation of R404a. The optimized ANFIS models report higher performance compared to the ANFIS model in terms of RMSE, R, and MAPE. ANFIS-GA model improves correlation coefficient for testing data as around 8% and decreases RMSE as approximately 52%. As can be seen in the table, the ANFIS-PSO model has the maximum correlation coefficient with R = 0.9876 and minimum RMSE and MAPE with 108.3395 and 1.35%, respectively for the testing datasets.

Table 4. A Comparison between the developed models.

	RMSE		R		MAPE	
Model	Train	Test	Train	Test	Train	Test
ANFIS	38.1079	346.5004	0.9985	0.9077	0.88%	6.12%
ANFIS-GA	149.9568	167.846	0.9812	0.9801	3.29%	1.82%
ANFIS-PSO	69.2325	108.3395	0.9960	0.9876	1.97%	1.35%

ANFIS-PSO model is applied to predict the HTC and is shown in Fig. 11. The graph shows the experimental HTC and its predicted values versus vapor quality for three values of mass flux (125, 156 and 188 kg/m^{2}s), curvature radius as 7.65 cm and pitch as 2.5 cm. The results show the proposed model (ANFIS-PSO) can successfully predict the HTC during condensation of R404a.

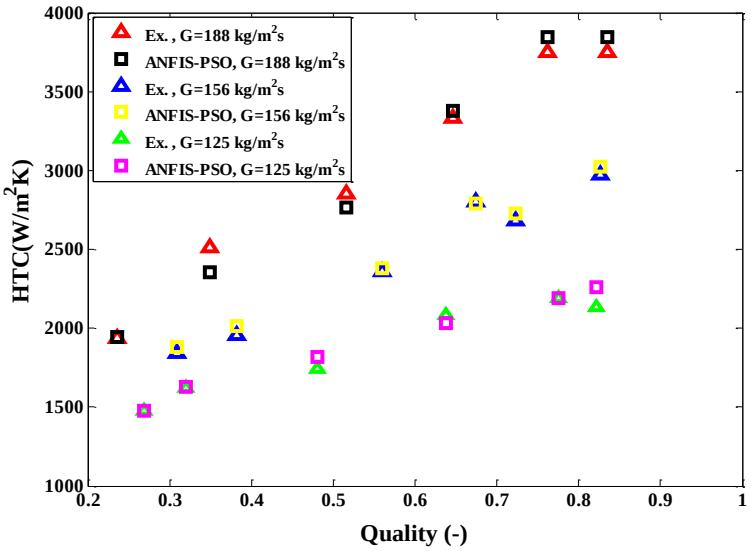

Figure 11. Using ANFIS-PSO to predict the HTC during condensation of R404a.

4. CONCLUSIONS

Determine the HTC during evaporation and condensation processes in refrigeration and air conditioning systems is a complex task compared to single-phase flow. Traditional correlations have proven to be inaccurate for this kind of processes, even though there is a need for good predictions in these applications. In this study, the ANFIS model was developed in order to predict HTC during condensation of R404a in a helically coiled tube. The results demonstrated that the ANFIS method predicted the HTC with correlation coefficient as 0.9985 for training phase of the network and 0.9077 for testing samples. It is clear that the predicted HTC for the new data (testing datasets) had more disagreement with the experimental data. Hence, GA and PSO optimization algorithms were applied in order to optimize the ANFIS model. The correlation coefficient that has been reported by ANFIS-GA improved around 8% compared to the ANFIS. Also, this model decreased approximately 52% the value of RMSE for testing datasets. Investigation of the results illustrated that the ANFIS-PSO has the maximum performance in terms of RMSE, R, and MAPE. The ANFIS-PSO model decreased RMSE for testing samples around 35% compared to the ANFIS-GA. Also, this model reported the maximum correlation coefficient and minimum MAPE for testing datasets as 0.9876 and 1.35%, respectively.

5. APPENDIX

5.1 Performance Evaluation Measures

Several evaluation criteria are applied to evaluate the performance of the developed models in terms of forecast accuracy. The mean absolute percentage error (MAPE) is a measure of prediction accuracy of a forecasting in statistics that is defined as follows:

$$MAPE = \frac{100}{n} \times \sum_{i=1}^{n} \left| \frac{x_i - y_i}{x_i} \right| \quad (1)$$

The coefficient of correlation (R) value is an indication of the relationship between the outputs and targets. If R = 1, this represents that there is an exact linear relationship between outputs and targets and R=0 illustrates that there is no linear relationship between outputs and targets.

$$R = \frac{\sum_{i=1}^{n}(x_i-\bar{x})(y_i-\bar{y})}{\sqrt{\sum_{i=1}^{n}(x_i-\bar{x})^2 \sum_{i=1}^{n}(y_i-\bar{y})^2}} \quad (2)$$

Root mean square error (RMSE) is the standard deviation of the prediction errors (targets-outputs).

$$RMSE = \sqrt{\frac{1}{n}\sum_{i=1}^{n}(x_i - y_i)^2} \quad (3)$$

Where x_i, y_i, $\bar{x}$, $\bar{y}$, and n are observed value, predicted value, mean of observed data, mean of predicted data, and number of data, respectively.

6. ACKNOWLEDGEMENTS

The authors gratefully acknowledge the support given by CAPES (Coordenação de Aperfeiçoamento de Pessoal de Nível Superior), CNPq (Conselho Nacional de Desenvolvimento Científico e Tecnológico) and FAPEMIG (Fundação de Amparo à Pesquisa do Estado de Minas Gerais).

7. REFERENCES

Azizi, S., Ahmadloo, E., 2016. Prediction of heat transfer coefficient during condensation of R134a in inclined tubes using artificial neural network. Appl. Therm. Eng. 106, 203–210.

Balachander, P., Raja, B., Lal, D.M., 2012. Evaporative heat transfer characteristics of R404A and R134a under varied heat flux conditions. Exp. Heat Transf. 25, 254–265.

Belman-Flores, J.M., Rodríguez-Muñoz, A.P., Pérez-Reguera, C.G., Mota-Babiloni, A., 2017. Experimental study of R1234yf as a drop-in replacement for R134a in a domestic refrigerator. Int. J. Refrig. 81, 1–11.

De Melo Reis, R.Vi., Oliviera, R.N., Machado, L., Koury, R.N.N., 2012. Using a heat pump as an alternative to support solar collector for water heating in Brazil. Int. J. Air-Conditioning Refrig. 20, 1250013.

Diani, A., Mancin, S., Rossetto, L., 2015. Flow boiling heat transfer of R1234yf inside a 3.4mm ID microfin tube. Exp. Therm. Fluid Sci. 66, 127–136.

Faria, R.N., Nunes, R.O., Koury, R.N.N., Machado, L., 2016. Dynamic modeling study for a solar evaporator with expansion valve assembly of a transcritical CO2 heat pump. Int. J. Refrig. 64, 203–213.

Gorenflo, D., Baumhögger, E., Herres, G., Kotthoff, S., 2014. Prediction methods for pool boiling heat transfer: A state-of-the-art review. Int. J. Refrig. 43, 203–226.

Goshayeshi, H.R., Khosravi, A., Karizaki, M.A., 2014. Experimental investigation on nanofluids effectiveness on heat transfer in oscillating heat pipe. Adv. Mater. Res. 856.

Guo, C., Wang, J., Du, X., Yang, L., 2016. Experimental flow boiling characteristics of R134a/R245fa mixture inside smooth horizontal tube. Appl. Therm. Eng. 103, 901–908.

Hassanpour, M., Vaferi, B., Masoumi, M.E., 2018. Estimation of pool boiling heat transfer coefficient of alumina water-based nanofluids by various artificial intelligence (AI) approaches. Appl. Therm. Eng. 128, 1208–1222.

Haznedar, B., Kalinli, A., 2016. Training ANFIS Using Genetic Algorithm for Dynamic Systems Identification. Int. J. Intell. Syst. Appl. Eng. 4, 44–47.

Huang, H., Thome, J.R., 2017. An experimental study on flow boiling pressure drop in multi-microchannel evaporators with different refrigerants. Exp. Therm. Fluid Sci. 80, 391–407.

Kumar, R., Kumar, P., 2016. Optimization of Heat Transfer Coefficient during Condensation of Refrigerant inside Plain Horizontal Tube using Teaching-Learning based Optimization Algorithm. Indian J. Sci. Technol. 9.

Ma, D., Zhou, T., Chen, J., Qi, S., Ali, M., Xiao, Z., 2017. Supercritical water heat transfer coefficient prediction analysis based on BP neural network. Nucl. Eng. Des. 320, 400–408.

Makhnatch, P., Mota-Babiloni, A., Khodabandeh, R., 2017. Experimental study of R450A drop-in performance in an r134a small capacity refrigeration unit. Int. J. Refrig.

Oliveira, M. V., Schirru, R., 2009. Applying particle swarm optimization algorithm for tuning a neuro-fuzzy inference system for sensor monitoring. Prog. Nucl. Energy 51, 177–183.

Quej, V.H., Almorox, J., Arnaldo, J.A., Saito, L., 2017. ANFIS, SVM and ANN soft-computing techniques to estimate daily global solar radiation in a warm sub-humid environment. J. Atmos. Solar-Terrestrial Phys. 155, 62–70.

Ren, T., Mu, H., Liu, S., Sun, Y., Zhang, J., Liu, S., 2017. Prediction of gas-liquid two-phase heat transfer coefficient.

Appl. Therm. Eng. 116, 217–232.
Romero-Méndez, R., Lara-Vázquez, P., Oviedo-Tolentino, F., Durán-García, H.M., Pérez-Gutiérrez, F.G., Pacheco-Vega, A., 2016. Use of Artificial Neural Networks for Prediction of the Convective Heat Transfer Coefficient in Evaporative Mini-Tubes. Ing. Investig. y Tecnol. 17, 23–34.
Salimpour, M.R., Shahmoradi, A., Khoeini, D., 2017. Experimental study of condensation heat transfer of R-404A in helically coiled tubes. Int. J. Refrig. 74, 584–591.
Sobhanifar, N., Ahmadloo, E., Azizi, S., 2015. Prediction of Two-Phase Heat Transfer Coefficients in a Horizontal Pipe for Different Inclined Positions With Artificial Neural Networks. J. Heat Transfer 137, 061009.
Wen, X.-L., Wang, H.-T., Wang, H., 2012. Prediction model of flow boiling heat transfer for R407C inside horizontal smooth tubes based on RBF neural network. Procedia Eng. 31, 233–239.

8. RESPONSIBILITY NOTICE

The authors are the only responsible for the printed material included in this paper.